
This copy is for your personal, non-commercial use only.

If you wish to distribute this article to others, you can order high-quality copies for your colleagues, clients, or customers by [clicking here](#).

Permission to republish or repurpose articles or portions of articles can be obtained by following the guidelines [here](#).

The following resources related to this article are available online at www.sciencemag.org (this information is current as of October 3, 2011):

Updated information and services, including high-resolution figures, can be found in the online version of this article at:

<http://www.sciencemag.org/content/333/6047/1307.full.html>

Supporting Online Material can be found at:

<http://www.sciencemag.org/content/suppl/2011/08/31/333.6047.1307.DC1.html>

A list of selected additional articles on the Science Web sites **related to this article** can be found at:

<http://www.sciencemag.org/content/333/6047/1307.full.html#related>

This article **cites 36 articles**, 11 of which can be accessed free:

<http://www.sciencemag.org/content/333/6047/1307.full.html#ref-list-1>

This article appears in the following **subject collections**:

Molecular Biology

http://www.sciencemag.org/cgi/collection/molec_biol

knockdown ES cells had little 5caC excision activity (Fig. 4D). Moreover, immunodepletion of TDG from the ES cell nuclear extract greatly reduced the 5caC excision activity (Fig. 4A, lane 3). These results indicate that TDG is able to recognize and excise 5caC, an oxidation product of 5mC, in duplex DNA.

Stable ES cell lines expressing a *Tdg*-specific small interfering RNA were established, and TDG depletion was confirmed by Western analysis (fig. S12). By using triple quadrupole mass spectrometry, we could detect 5caC in genomic DNA isolated from TDG-depleted ES cells, but no reliable signal was detected in TDG-proficient control cells expressing scramble short hairpin RNA (shRNA) (Fig. 4E). Similarly, 5caC was detectable in mouse induced pluripotent stem (iPS) cells when the *Tdg* gene was knocked out (fig. S13). Judging from our calculation based on the measurement of a 5caC standard, the number of 5caC per genome is ~9000 in *Tdg*-depleted ES or iPS cells but below 1000 in wild-type cells.

TDG has been implicated in DNA demethylation for its function in excising the deamination product of 5mC, 5hmC, or 5mC itself from DNA (17–19), yet mammalian TDG lacks glycosylase activity toward 5mC (6, 12). Although TDG is able to excise 5hmU (19), the deamination product of 5hmC, our work provides evidence that the Tet dioxygenases oxidize 5mC and 5hmC to 5caC, which becomes a substrate for TDG. Therefore, Tet-mediated conversion of 5mC and 5hmC to 5caC could trigger TDG-initiated BER, as indicated here. These sequential events would lead to DNA demethylation, because unmethylated cytosines are inserted into the repaired genomic region (fig. S14).

Genome-wide mapping revealed that Tet1 is relatively enriched in CpG-rich active promoters that are unmethylated (20–23), but 5hmC is underrepresented in the majority of Tet1 binding sites in ES cells (24–26). These apparent paradoxes might be accounted for if active promoters with Tet1 binding sites were prevented from erroneous hypermethylation because of Tet1 oxidizing 5mC into 5caC, which could then be removed by TDG-mediated BER repair. In this case, 5mC is most likely undetectable in the active promoters because of their transient existence in a small proportion of cells. Likewise, in many of the Tet1 binding sites, 5hmC could be underrepresented because of conversion to 5caC, which is rapidly removed in cells.

Note added in proof: During the revision of this manuscript, Ito *et al.*'s report (www.sciencemag.org/content/early/2011/07/20/science.1210597.abstract) appeared online describing the enzymatic activity of Tet proteins in the conversion of 5mC to 5fC and 5caC, as well as the detection of these derivatives in mouse genomic DNA.

References and Notes

- R. Jaenisch, A. Bird, *Nat. Genet.* **33** (suppl.), 245 (2003).
- S. Simonsson, J. Gurdon, *Nat. Cell Biol.* **6**, 984 (2004).
- X. J. He, T. Chen, J. K. Zhu, *Cell Res.* **21**, 442 (2011).
- Z. Liutkeviciute, G. Lukinavicius, V. Masevicius, D. Daujotyte, S. Klimasauskas, *Nat. Chem. Biol.* **5**, 400 (2009).
- C. P. Walsh, G. L. Xu, *Curr. Top. Microbiol. Immunol.* **301**, 283 (2006).
- S. C. Wu, Y. Zhang, *Nat. Rev. Mol. Cell Biol.* **11**, 607 (2010).
- C. Dahl, K. Grønbaek, P. Guldborg, *Clin. Chim. Acta* **412**, 831 (2011).

- M. Tahiliani *et al.*, *Science* **324**, 930 (2009).
- T. Pfaffeneder *et al.*, *Angew. Chem. Int. Ed. Engl.* **50**, 7008 (2011).
- D. Globisch *et al.*, *PLoS ONE* **5**, e15367 (2010).
- T. Lindahl, R. D. Wood, *Science* **286**, 1897 (1999).
- D. Cortázar *et al.*, *Nature* **470**, 419 (2011).
- M. T. Bennett *et al.*, *J. Am. Chem. Soc.* **128**, 12510 (2006).
- B. Hendrich, U. Hardeland, H. H. Ng, J. Jiricny, A. Bird, *Nature* **401**, 301 (1999).
- H. E. Krokan, R. Standal, G. Slupphaug, *Biochem. J.* **325**, 1 (1997).
- R. J. Boorstein *et al.*, *J. Biol. Chem.* **276**, 41991 (2001).
- R. Métiévier *et al.*, *Nature* **452**, 45 (2008).
- B. Zhu *et al.*, *Proc. Natl. Acad. Sci. U.S.A.* **97**, 5135 (2000).
- S. Cortellino *et al.*, *Cell* **146**, 67 (2011).
- W. A. Pastor *et al.*, *Nature* **473**, 394 (2011).
- G. Ficz *et al.*, *Nature* **473**, 398 (2011).
- C. X. Song *et al.*, *Nat. Biotechnol.* **29**, 68 (2011).
- H. Wu *et al.*, *Genes Dev.* **25**, 679 (2011).
- K. Williams *et al.*, *Nature* **473**, 343 (2011).
- Y. Xu *et al.*, *Mol. Cell* **42**, 451 (2011).
- H. Wu *et al.*, *Nature* **473**, 389 (2011).

Acknowledgments: We thank C. Walsh for critical reading of the manuscript, G. Shi and S. Klimasauskas for discussions, J. Ju for providing Tet cDNA clones, T. Carell for 2'-deoxy-5-carboxylcytidine and Z. Hua for the TDG antibody. This study was supported by grants from the Ministry of Science and Technology China (2007CB947503 and 2009CB941101 to G.-L.X., 2010CB912100 to L.L.), National Science Foundation of China (30730059 to G.-L.X., 30930052 and 30821065 to L.L.), and the Strategic Priority Research Program of the Chinese Academy of Sciences (XDA01010301 to G.-L.X.) and by the NIH (GM071440 to C.H.) and (1510RR027643-01 to K.Z.).

Supporting Online Material

www.sciencemag.org/cgi/content/full/science.1210944/DC1
Materials and Methods
Figs. S1 to S14
References (27–32)

11 July 2011; accepted 25 July 2011
Published online 4 August 2011;
10.1126/science.1210944

Multi-Input RNAi-Based Logic Circuit for Identification of Specific Cancer Cells

Zhen Xie,^{1,2*} Liliana Wroblewska,² Laura Prochazka,³ Ron Weiss,^{2,4†} Yaakov Benenson^{1,3,††}

Engineered biological systems that integrate multi-input sensing, sophisticated information processing, and precisely regulated actuation in living cells could be useful in a variety of applications. For example, anticancer therapies could be engineered to detect and respond to complex cellular conditions in individual cells with high specificity. Here, we show a scalable transcriptional/posttranscriptional synthetic regulatory circuit—a cell-type “classifier”—that senses expression levels of a customizable set of endogenous microRNAs and triggers a cellular response only if the expression levels match a predetermined profile of interest. We demonstrate that a HeLa cancer cell classifier selectively identifies HeLa cells and triggers apoptosis without affecting non-HeLa cell types. This approach also provides a general platform for programmed responses to other complex cell states.

Synthetic biomolecular pathways with elaborate information processing capability will enable in situ response to complex physiological conditions (1). For example, mul-

multiple cancer-specific biomarkers (2) can be sensed and integrated in such pathways, providing precise control of therapeutic agents (3). A combination of up to two tissue-specific signals, including

promoter and/or microRNA (miRNA) activity, mRNA, and protein levels, have been used to partially restrict therapeutic action to cancer cells (4–9). In parallel, research in synthetic biology has demonstrated multi-input information processing in living cells (10–18), but the interaction between these systems and the cellular context has been limited. Yet, general-purpose mechanisms for programmable integration of multiple markers are required to detect cell state and precisely

¹Faculty of Arts and Sciences (FAS) Center for Systems Biology, Harvard University, 52 Oxford Street, Cambridge, MA 02138, USA. ²Department of Biological Engineering, Massachusetts Institute of Technology (MIT), 40 Ames Street, Cambridge, MA 02142, USA. ³Department of Biosystems Science and Engineering, Eidgenössische Technische Hochschule (ETH) Zürich, Mattenstrasse 26, Basel 4058, Switzerland. ⁴Department of Electrical Engineering and Computer Science, MIT, 40 Ames Street, Cambridge MA 02142, USA.

*Present address: Department of Biological Engineering, MIT, 40 Ames Street, Cambridge, MA 02142, USA.

†To whom correspondence should be addressed. E-mail: kobi.benenson@bsse.ethz.ch (Y.B.); rweiss@mit.edu (R.W.)

††Present address: Department of Biosystems Science and Engineering, ETH Zürich, Mattenstrasse 26, Basel 4058, Switzerland.

regulate therapeutic actuation. Here, we describe such a mechanism, a “classifier” gene circuit that integrates sensory information from a large number of molecular markers to determine whether a cell is in a specific state and, if so, produces a biologically active protein output. Specifically, when transiently expressed inside a cell our classifier ascertains whether the expression profile of six endogenous miRNAs (19) matches a predetermined reference profile characteristic of the HeLa cervical cancer cell line. A match identifies the cell as HeLa and triggers apoptosis (Fig. 1A).

A HeLa reference profile was constructed by choosing a set of HeLa-high and HeLa-low markers so that HeLa cells express high or low levels of these, respectively, whereas expression in any healthy cell differs substantially from that of a typical HeLa cell for at least one of these markers. Multiple reference profiles are possible, and these profiles do not need to differentiate HeLa from other cancers. We designed a sensor motif for HeLa-high markers comprising a “double-inversion” module that allows output expression only if the marker is present at or above its level in HeLa cells but efficiently represses the output if the marker’s level is low. The design is based on our previously described module that consists of the small interfering RNA (siRNA)-targeted transcriptional Lac repressor (LacI) and a LacI-controlled promoter CAGop (CAG promoter followed by an intron with two LacO sites) (17). We improved the ON:OFF ratio of our original design to approximately 8- to

10-fold by introducing a reverse tetracycline-controlled transactivator (rtTA) to control LacI and by targeting both the repressor and the activator using miRNA in a feed-forward loop (Fig. 1B and fig. S1) (20, 21). A HeLa-low marker sensor was implemented by fusing four repeats (5) of fully complementary target sites into the output’s 3′-untranslated region (3′-UTR) (Fig. 1C). A complete classifier circuit consists of a set of HeLa-high and HeLa-low marker sensors all arranged to target the same output (Fig. 1D). Multiple HeLa-low sensors are combined by fusing their corresponding miRNA targets in the output’s 3′-UTR (17). Multiple HeLa-high sensors are integrated by regulating the same output in parallel. Accordingly, all HeLa-high markers must be present at the same time to enable output expression from CAGop because any individual double-inversion module can efficiently repress the output by itself (22).

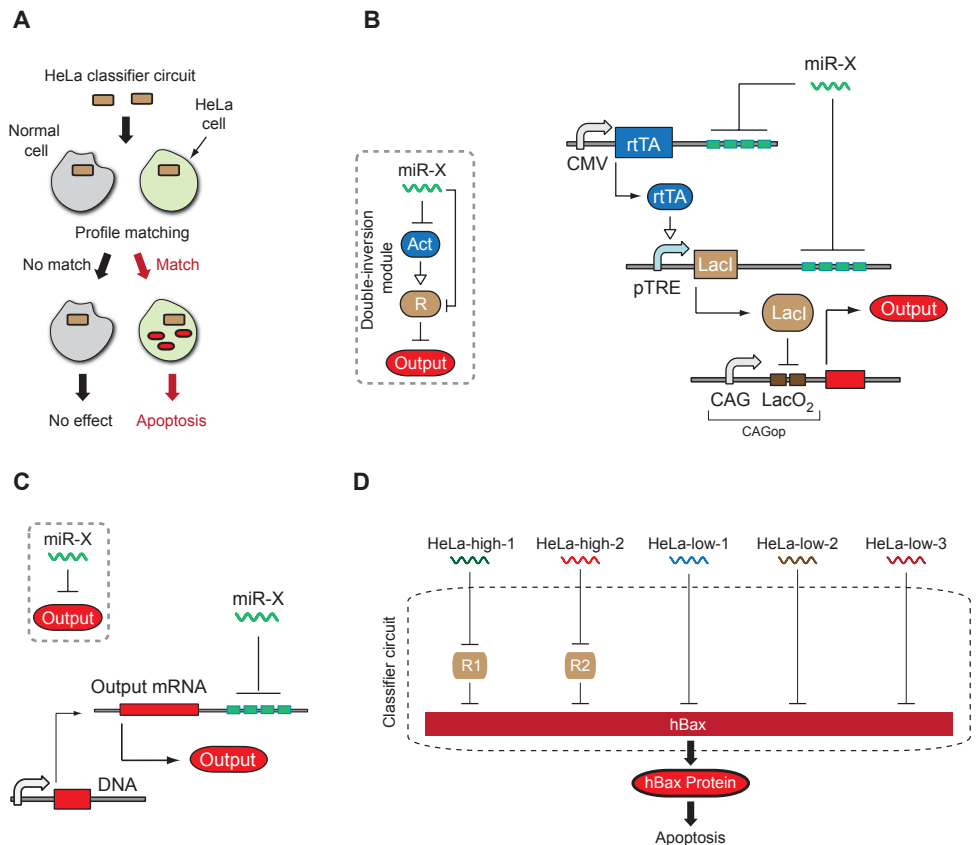
To choose HeLa markers for the reference profile and analyze expected circuit performance, we created a mathematical model consisting of a multi-variable circuit response function that uses experimentally derived responses (23) of individual sensors to their miRNA inputs [fig. S2 and supporting online material (SOM) text]. We first evaluated HeLa-high marker combinations from the set of the top 12 candidates determined by analyzing expression data from the MicroRNA Atlas (fig. S3) (24). On the basis of reasonable assumptions regarding sensor response parameters (22), we found that using miR-21 together

with a composite marker that includes both miR-17 and miR-30a (miR-17-30a) results in at least a fivefold difference between circuit output in HeLa cells and the output in all but a few healthy cell types profiled in the MicroRNA Atlas (Fig. 2A and fig. S2D) (24). We then searched for HeLa-low markers and found that miR-141, miR-142(3p), and miR-146a are highly expressed in the potentially misclassified cell types but unexpressed in HeLa (Fig. 2B). With inclusion of these inputs in the response function, the model predicts at least a sixfold output difference in HeLa cells relative to the closest other cell type USSC-7d and on average about a 160-fold difference relative to the rest of the cells (fig. S2E). We also computed selectivity of all possible marker subsets and found that it steadily increases as the number of markers goes from one to five (Fig. 2C). With all inputs included, the response function is well approximated by a Boolean expression (fig. S2F):

$$\begin{aligned} & \text{miR-21 AND miR-17-30a} \\ & \text{AND NOT(miR-141)} \\ & \text{AND NOT[miR-142(3p)]} \\ & \text{AND NOT(miR-146a)} \end{aligned}$$

In addition to HeLa, we tested circuit operation in six control cell lines. For practical reasons, most of these are cancer cell lines that can be handled with ease and that are predicted by the model to produce less than 1% of HeLa output (22, 24). First, we measured all miRNA activities

Fig. 1. High-level architecture of a cell type classifier. **(A)** Schematic representation of a HeLa-specific classifier circuit operation. Gray circle, healthy cells; light green, HeLa cells. **(B)** High-level and detailed description of double-inversion module for sensing HeLa-high miRNAs. Act, activator; R, repressor. **(C)** High-level and detailed description of HeLa-low miRNA sensor. **(D)** Schematic representation of an integrated multi-input classifier. Lines with bars indicate down-regulation. R1 and R2 represent double-inversion modules. The entire network implements a multi-input AND-like logic function for identification and selective killing of HeLa cells through regulated expression of hBax.



and HeLa-high sensor responses (Fig. 2D and fig. S4). For the HeLa-high sensors, we found a qualitatively correct relationship between miRNA activity and the output of the double-inversion modules (fig. S5A). We also observed that the combined effect of all three HeLa-low sensors is generally stronger than a simple prediction according to individually measured miRNA activities (fig. S5B).

Next, we validated the response of the complete circuit (Fig. 2E) in HeLa cells by systematically modulating all inputs and measuring the output for a total of $2^5 = 32$ combinations of ON and OFF inputs (fig. S6). Although the results generally agree with expectation in all 32 cases, we detected undesirably high output levels in the three conditions in which one of the HeLa-high markers and all HeLa-low markers were set to OFF. To reduce this leakiness, we introduced in a HeLa-high sensor an additional posttranscriptional repression element by engineering intronic miRNA to coexpress with LacI (25, 26), improving the

worst case ON:OFF ratio of the circuit from approximately 4- to ~10-fold (Fig. 2F and fig. S7).

Subsequently, we tested subcircuits of increasing complexity in the different cell lines (Fig. 3A and figs. S8 and S9). In any cell line, the upper bound on circuit output is obtained when a red fluorescent protein DsRed is constitutively expressed from unrepressed CAGop promoter, whereas the lower bound is obtained when DsRed is repressed by fully active double-inversion modules and endogenous HeLa-low markers. Constitutive CAGop expression varies widely among the cell lines (Fig. 3A, top row), but repression was uniformly efficient (Fig. 3A, middle row). For CAGop-driven DsRed with the three HeLa-low sensors (“all-low” circuit), and an “all-high” circuit with only HeLa-high sensors, output expression levels normalized to the output upper bound in each cell line (fig. S8) were generally consistent with expectation. In the all-low circuits, in many cases we actually observed an improvement over a simple prediction based on indi-

vidual miRNA activities (fig. S5C). In all-high circuits, the performance seems to reflect an additive function of the individual sensor responses (fig. S5D), suggesting that the circuit operates in a gradual fashion in at least some of the cell lines. Despite occasional deviations of subcircuit behavior from simple computational predictions, the complete circuit performs as desired experimentally, resulting in an output that is substantially higher in HeLa cells both in absolute and relative units as compared with the other cell lines in the set (Fig. 3A, bottom row, and fig. S5E). Analysis reveals that for the cell types assayed, the circuit operates well because of one of two conditions: At least one sensor exhibits a response in a non-HeLa cell that is an inverse of that sensor’s response in a HeLa cell [human embryonic kidney (HEK) 293, MCF-7, and SH-SY5Y], or a sufficient number of responses deviate moderately from the ones observed in HeLa cells (DAOY, SKBR3, and T47D). The classifier’s output in T47D is much better than the prediction,

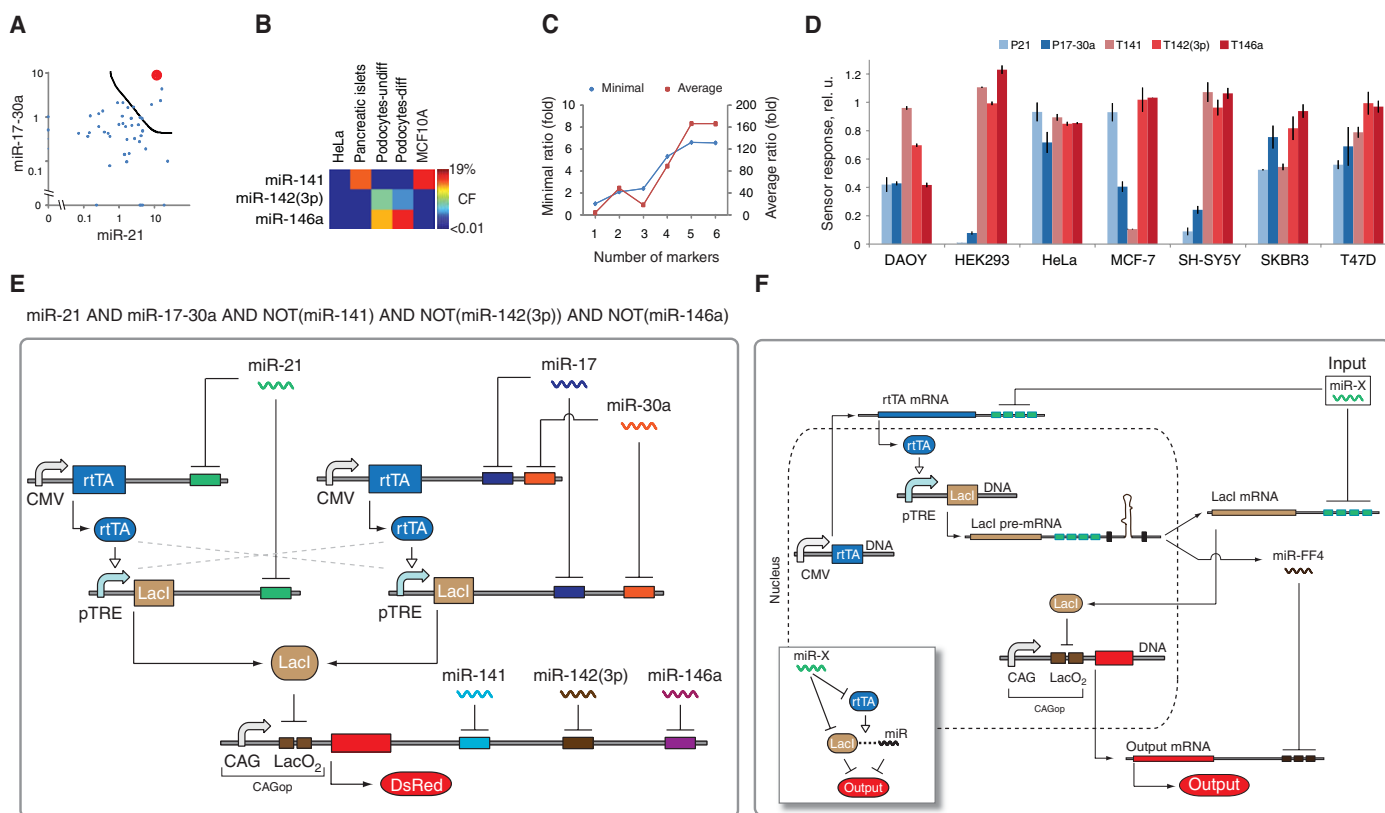


Fig. 2. Design of HeLa classifier. (A) Simulated output levels of a two-input circuit with miR-21 and miR-17-30a inputs. Each dot represents a particular cell type, and the contour line shows input combinations that result in 20% output relative to HeLa cells (red dot). Dots above the contour line represent “false-positive” cell types for this specific circuit configuration. The numbers on the axes are given in cloning frequency (CF) units. (B) CF of selected HeLa-low markers in false-positive cell types. (C) Circuit selectivity as a function of the number of markers. For a given number of markers (*x* axis), we computationally generate all possible classifier circuits by choosing subsets of markers from the set of six chosen markers and evaluate circuit output in HeLa cells and in the profiled healthy cell types. We then choose a circuit that maximizes the worst output ratio between HeLa and all non-HeLa

cell types (“minimal”) and also calculate the average output ratio for this circuit (“average”). (D) miRNA marker sensor responses in different cell lines (tables S1 and S3). Bars show mean \pm SD of normalized sensor output measured in three independent flow cytometry experiments (fig. S4). (E) Schematics of the complete classifier circuit. For simplicity, four adjacent miRNA target sites are shown as a wider box, and DNA/RNA species are lumped together. Two double-inversion modules for HeLa-high markers and three sensors for HeLa-low markers are shown. rtTA crosstalk is indicated with dotted lines. The logic “computed” by the circuit is shown on top. (F) Optimized sensor configuration for HeLa-high markers. (Inset) Simplified network diagram of the sensing process. miR-FF4 is a synthetic microRNA co-transcribed with LacI.

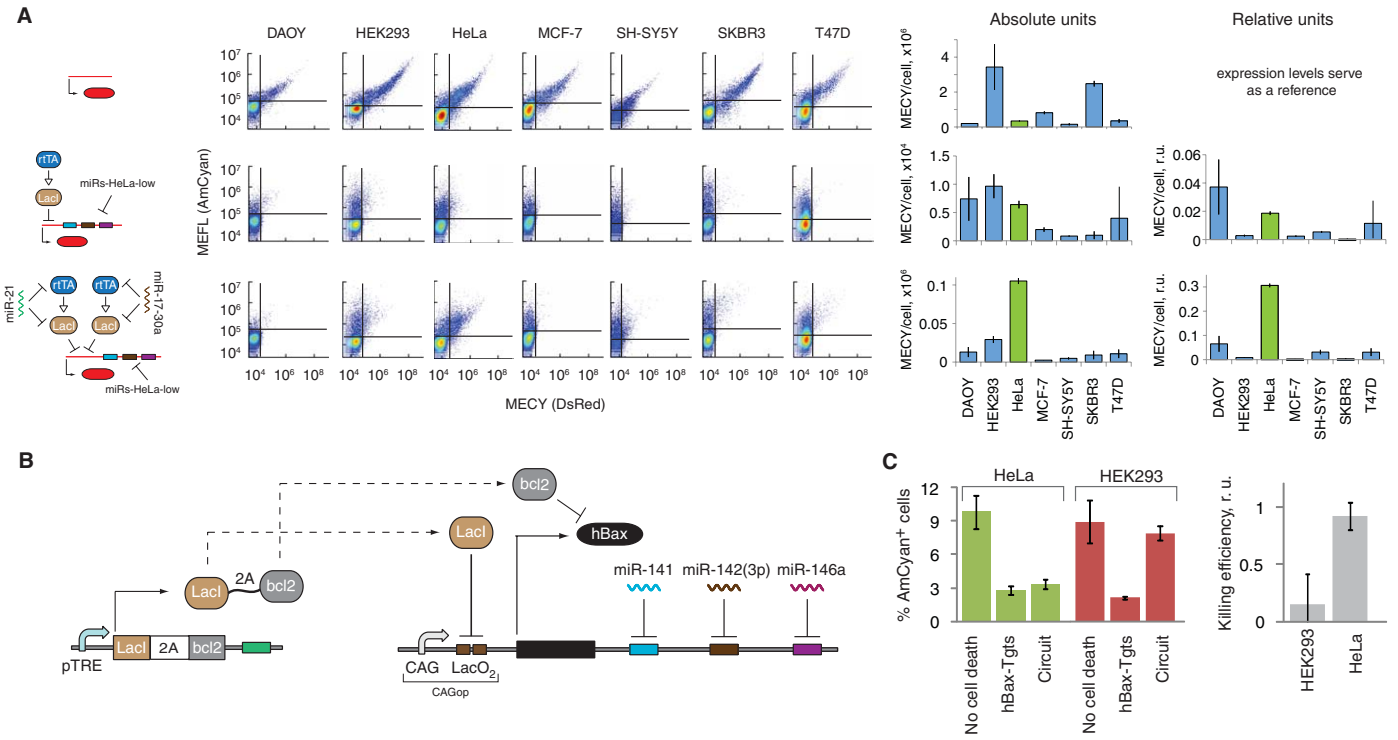
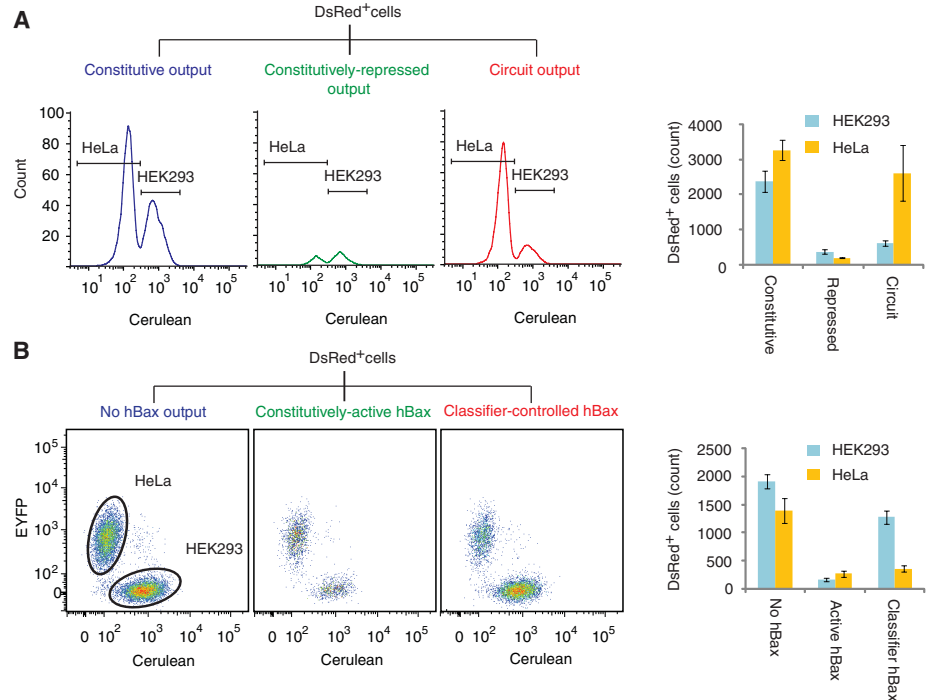


Fig. 3. The classifier circuit identifies and specifically kills HeLa cells (tables S3A and S3B). **(A)** Fluorescence reporter assays. (Left to right) Schematics of tested circuits, representative flow cytometry scatter plots, and absolute and relative output levels. Each bar shows mean \pm SD from at least three independent replicates (22). **(B)** Modifications to the circuit for apoptotic protein output, in which DsRed is replaced with a gene for hBax protein. LacI protein is cotranslated with an hBax inhibitor bcl2 by using a 2A linker (only one LacI construct is shown). **(C)** Apoptosis assays in HeLa and HEK293 cell lines. The CAG-AmCyan transfection marker

indicates cell survival. AmCyan⁺ fraction—percentage of AmCyan-positive cells gated using untransfected cells as a reference (fig. S8)—was measured 4 days after transfection by means of fluorescence-activated cell sorting (FACS). “No cell death” indicates cells cotransfected with an all-low circuit with a DsRed output. hBax-Tgts, cells cotransfected with an all-low circuit with a hBax output; circuit, complete classifier circuit. Each bar represents mean \pm SD of the AmCyan⁺ fraction from three independent replicates. (Right) Comparison of the circuit-killing efficiency for HEK293 versus HeLa cells (22).

Fig. 4. Fluorescent reporter assays and killing experiments in cell mixtures (table S4). **(A)** Fluorescent reporter assays. The histograms show the fractions of HeLa and HEK-Cerulean in the DsRed⁺ cell population. The bar chart shows the absolute numbers of DsRed⁺ cells (mean \pm SD) under the indicated conditions. **(B)** Apoptotic assays in cell mixture. The scatter plots show the fractions of HeLa-EYFP and HEK293-Cerulean cells among the DsRed⁺ cell population interpreted as surviving transfected cells. The bar chart shows the absolute number of surviving HEK293 and HeLa DsRed⁺ cells (mean \pm SD) under the indicated conditions.



suggesting that further model refinement may be necessary.

Lastly, we tested whether the circuit can selectively trigger apoptosis by regulating expression of human Bcl-2-associated X protein hBax (27). Because constitutive expression of hBax resulted in efficient killing only in HeLa and HEK293 cells, we chose to focus on this pair. To quantify circuit-induced cell death (5), constitutively expressed cyan fluorescent protein (AmCyan) transfection/survival reporter and the apoptosis-inducing classifier (Fig. 3B) were cotransfected into cells. We observed that among transfected cells, apoptosis-inducing classifier circuit inflicts almost the same degree of cell death in HeLa cells as does constitutively expressed hBax but causes little cell death in HEK293 cells, indicating selective actuation (Fig. 3C).

An important measure of circuit performance is specificity and selectivity in heterogeneous cell populations. Cocultured fluorescent HEK293-Cerulean cells (22) and unmodified HeLa cells were transfected with various circuits expressing DsRed output (Fig. 4A and figs. S10 and S11A). In the mixture transfected with the complete circuit, the DsRed⁺ population was strongly biased toward HeLa cells relative to the control, as expected. To test selective induction of HeLa cell death in a cell mixture, CAG-driven transfection/survival reporter DsRed was cotransfected with the apoptosis-inducing classifier to cocultured HEK293-Cerulean and HeLa-EYFP cells (Fig. 4B and fig. S11B) (22). The classifier with hBax results in markedly stronger apoptosis of transfected HeLa-EYFP cells compared with HEK293-Cerulean cells. Taken together, the results confirm that programmed detection and apoptosis of HeLa cells operate correctly in a cell mixture. However, the observed degree of false-positive cell detection and cell death as well as false-negative cell survival warrants continuing circuit optimization. In part, it can be explained by high circuit output in HEK293 cells due to high CAGop activity in these cells relative to HeLa that could be alleviated by using a constitutive promoter with more uniform activity in different cell lines.

We show that synthetic biological networks and potentially their combinations (fig. S12) can trigger programmed biological actuation when complex intracellular conditions are detected. The results suggest potential therapeutic usage for the circuit, provided that challenges such as efficient *in vivo* DNA delivery to cells (28) are overcome. At the same time, *in vitro* applications that include drug screening or monitoring of developmental processes may be enabled in the near term by means of stable integration of classifier circuit into cultured cells. In addition, our engineered convergent and divergent control by miRNA together with complex interactions between miRNA and transcription factors validates recently suggested endogenous roles of miRNA

in regulatory pathways (29, 30). Such synthetic transcriptional/posttranscriptional gene circuits will continue to be complementary to existing tools for elucidating mechanisms of natural biological processes.

References and Notes

1. E. Shapiro, Y. Benenson, *Sci. Am.* **294**, 44 (2006).
2. T. R. Golub *et al.*, *Science* **286**, 531 (1999).
3. Y. Benenson, B. Gil, U. Ben-Dor, R. Adar, E. Shapiro, *Nature* **429**, 423 (2004).
4. J. H. Mansfield *et al.*, *Nat. Genet.* **36**, 1079 (2004).
5. B. D. Brown *et al.*, *Nat. Biotechnol.* **25**, 1457 (2007).
6. C. Wu *et al.*, *Mol. Ther.* **17**, 2058 (2009).
7. C. Y. Lee, P. S. Rennie, W. W. Jia, *Clin. Cancer Res.* **15**, 5126 (2009).
8. S. J. Culler, K. G. Hoff, C. D. Smolke, *Science* **330**, 1251 (2010).
9. S. Venkataraman, R. M. Dirks, C. T. Ueda, N. A. Pierce, *Proc. Natl. Acad. Sci. U.S.A.* **107**, 16777 (2010).
10. M. B. Elowitz, S. Leibler, *Nature* **403**, 335 (2000).
11. V. J. Martin, D. J. Pitera, S. T. Withers, J. D. Newman, J. D. Keasling, *Nat. Biotechnol.* **21**, 796 (2003).
12. S. Basu, Y. Gerchman, C. H. Collins, F. H. Arnold, R. Weiss, *Nature* **434**, 1130 (2005).
13. S. Hooshangi, S. Thiberge, R. Weiss, *Proc. Natl. Acad. Sci. U.S.A.* **102**, 3581 (2005).
14. M. N. Win, C. D. Smolke, *Science* **322**, 456 (2008).
15. A. E. Friedland *et al.*, *Science* **324**, 1199 (2009).
16. T. Danino, O. Mondragón-Palominó, L. Tsimring, J. Hasty, *Nature* **463**, 326 (2010).
17. K. Rinaudo *et al.*, *Nat. Biotechnol.* **25**, 795 (2007).
18. M. Leisner, L. Bleris, J. Lohmueller, Z. Xie, Y. Benenson, *Nat. Nanotechnol.* **5**, 666 (2010).
19. D. P. Bartel, *Cell* **136**, 215 (2009).
20. S. Mangan, U. Alon, *Proc. Natl. Acad. Sci. U.S.A.* **100**, 11980 (2003).
21. A. Re, D. Corá, D. Taverna, M. Caselle, *Mol. Biosyst.* **5**, 854 (2009).
22. Materials and methods are available as supporting material on Science Online.
23. M. Miyagishi, M. Hayashi, K. Taira, *Antisense Nucleic Acid Drug Dev.* **13**, 1 (2003).
24. P. Landgraf *et al.*, *Cell* **129**, 1401 (2007).
25. T. L. Deans, C. R. Cantor, J. J. Collins, *Cell* **130**, 363 (2007).
26. D. Greber, M. D. El-Baba, M. Fussenegger, *Nucleic Acids Res.* **36**, e101 (2008).
27. S. L. Lowe *et al.*, *Gene Ther.* **8**, 1363 (2001).
28. J. J. Green, R. Langer, D. G. Anderson, *Acc. Chem. Res.* **41**, 749 (2008).
29. M. E. Peter, *Oncogene* **29**, 2161 (2010).
30. E. Hornstein, N. Shomron, *Nat. Genet.* **38** (suppl.), S20 (2006).

Acknowledgments: We thank M. Leisner, J. Lohmueller, L. Bleris, and the members of FAS Center for Systems Biology for discussions; G. Winer for critical reading of the manuscript; and M. Leisner for CAGop-ZsYellow plasmid. We thank B. Tilton, P. Rogers, and G. Paradis for assistance with flow cytometry. The research was funded by the Bauer Fellows program, the National Institute of General Medical Sciences grant GM068763 for National Centers of Systems Biology, U.S. Army Congressionally Directed Medical Research Programs grant W81XWH-09-1-0240 BC085163, National Cancer Institute grant 1R01CA155320-01, and ETH Zürich core funding. Y.B., Z.X., and R.W. conceived of the ideas implemented in this study. Z.X. performed most of the experiments and data analysis. L.W. constructed stable, cell lines and performed experiments with MCF-7 cells and initial testing of the hBax protein and the 2A linker. L.P. performed experiments and data analysis in HEK293, HeLa, and T47D cells. Y.B. and R.W. supervised the project and performed data analysis. Y.B., Z.X., and R.W. wrote the paper. Raw and processed data are stored on our laboratory servers and are available upon request. A U.S. patent concerning the technology described in this paper has been filed by Harvard University and MIT entitled "Multiple Input Biologic Classifier Circuits for Cells."

Supporting Online Material

www.sciencemag.org/cgi/content/full/333/6047/1307/DC1
Materials and Methods
SOM Text
Figs. S1 to S13
Tables S1 to S6
References (31–37)

14 March 2011; accepted 15 July 2011
10.1126/science.1205527

Epigenetic Licensing of Germline Gene Expression by Maternal RNA in *C. elegans*

Cheryl L. Johnson and Andrew M. Spence*

RNA can act as a regulator of gene expression with roles in transposon silencing, antiviral defense, and cell fate determination. Here, we show that in *Caenorhabditis elegans* a maternal transcript of the sex-determining gene *fem-1* is required to license expression of a wild-type *fem-1* allele in the zygotic germ line. Females homozygous for *fem-1* deletions produce heterozygous offspring exhibiting germline feminization, reduced *fem-1* activity, and transcript accumulation. Injection of *fem-1* RNA incapable of encoding a protein into the maternal germ line rescues this defect in the progeny. The defect in zygotic *fem-1* expression is heritable, suggesting that the gene is subject to epigenetic silencing that is prevented by maternal *fem-1* transcripts. This mechanism may contribute to protecting the identity and integrity of the germ line.

In *Caenorhabditis elegans*, sex is determined by the X chromosome:autosome ratio, which directs diploid animals with one X chromosome (XO) to develop as males and those with

two X chromosomes (XX) to become self-fertile hermaphrodites (1). The *fem-1* gene is required for male development in both males and hermaphrodites (2). Animals that lack both maternal